Article

Revealing the Structural, Elastic, Electronic, and Optical Properties of K$_2$ScCuCl$_6$ and K$_2$YCuCl$_6$: An In-Depth Exploration Using Density Functional Theory

Saima Ahmad Shah, Mudasser Husain, Nasir Rahman,* Nourreddine Sfina, Muawya Elhadi,
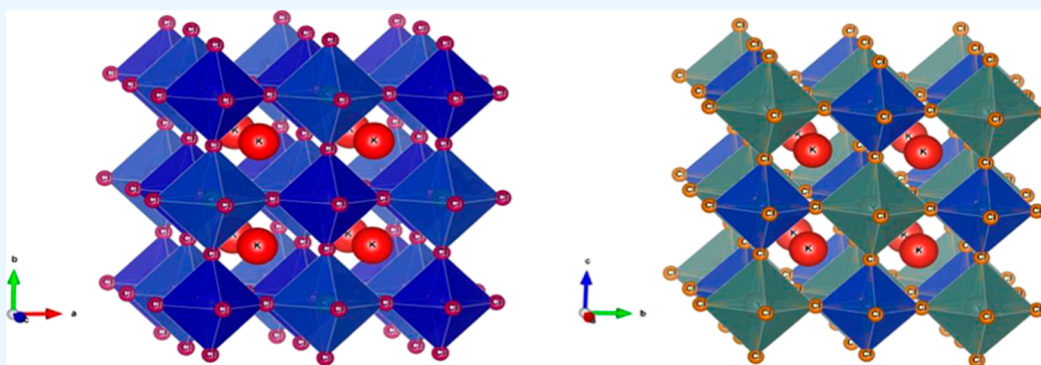Vineet Tirth, Afraa Alotaibi, and Aurangzeb Khan*

Read Online

ACCESS | 📊 Metrics & More | 📰 Article Recommendations

ABSTRACT: The optoelectronic, structural, and elastic properties of K$_2$ScCuCl$_6$ and K$_2$YCuCl$_6$ double perovskite compounds were thoroughly investigated in this study using density functional theory. It is observed that both compounds exhibit exceptional structural and mechanical stability. The structural stability is assessed using Goldsmith's tolerance factor (t_G), with values approaching unity indicating a reliable cubic perovskite structure. Phonon stability was ensured by the absence of negative energy formations and only real frequencies in the phonon calculations. Applying the finite displacement method also provided further evidence of the compounds' thermodynamic stability. The electronic properties analysis revealed that K$_2$ScCuCl$_6$ and K$_2$YCuCl$_6$ are narrow band gap semiconductors, with band gap values of 1.8 and 2.5 eV, respectively. This was confirmed by analyzing the density of states. Furthermore, the optical properties exhibited transparency at lower photon energies and significant absorption at higher energies. These exciting findings suggest that K$_2$ScCuCl$_6$ and K$_2$YCuCl$_6$ have promising applications in high-frequency UV devices.

1. INTRODUCTION

In today's world, the global energy crisis, coupled with the persistent issues of global warming and the limited availability of fossil fuels, necessitates a shift toward renewable energy sources and advancements in energy conversion and storage technologies.[1−3] While numerous options exist, not all of them are economically feasible. Fortunately, a significant portion of the world benefits from abundant sunlight throughout the year, making solar energy an attractive and potentially cost-effective solution to the energy crisis while providing clean and affordable power.[4,5] However, developing cost-effective and efficient solar cells remains challenging and requires ongoing research and innovation.[6,7] The key to achieving such solar cells lies in understanding the properties and characteristics of the materials used and the design approaches employed for their fabrication.[8] However, the cost-effectiveness and efficiency of solar cells are critical factors in determining their widespread adoption.[9] The development of solar cell technology involves addressing multiple challenges, including improving the conversion efficiency of sunlight into electricity, reducing manufacturing costs, enhancing durability and stability, and optimizing the materials and design of the solar cell itself.[10,11] The characteristics of the materials used in solar cells play a crucial role in determining their performance.[12] One promising class of materials for solar cell applications is double perovskites. Double perovskites are compounds composed of two transition-metal cations arranged in a perovskite crystal structure.[13−15] These materials exhibit unique electronic and optical properties that can be tailored to enhance the efficiency and cost-effectiveness
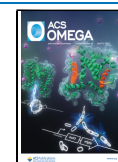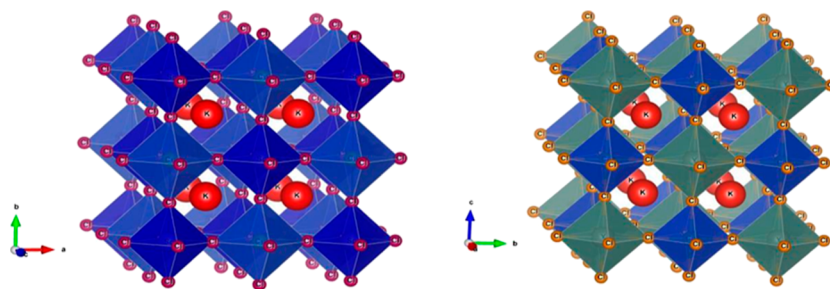
Figure 1. Schematic 3D-crystalline structure of $K_2ScCuCl_6$ and K_2YCuCl_6 double perovskite compounds.

Table 1. Optimized Unit Cell Parameters and Atomic Positions

compounds	a_0 (Å)/b_0 (Å)/c_0 (Å)	$\alpha/\beta/\gamma$	K (x, y, z)	Sc/Y (x, y, z)	Cu (x, y, z)	Cl (x, y, z)
$K_2ScCuCl_6$	10.25	90°	(1/4, 3/4, 3/4)	(0, 0, 0)	(1/2, 0, 0)	(0.24, 0, 0)
K_2YCuCl_6	10.30	90°	(1/4, 3/4, 3/4)	(0, 0, 0)	(1/2, 0, 0)	(0.274, 0, 0)

of solar cells.[16] By understanding solar cells' materials and design aspects, particularly those based on double perovskites, we aim to contribute to advancing solar cell technology, bringing us closer to achieving affordable and efficient solar energy conversion.[17,18] The conversion of solar energy into electrical energy has seen significant advancements, with the emergence of organic−inorganic perovskite materials. Among these, the Pb-based compounds, e.g., $CH_3NH_3PbX_3$ (X = I, Br, and Cl), have demonstrated remarkable efficiency, reaching up to 22.1%. However, these materials present two main limitations: instability under ambient conditions and toxicity due to Pb.[19] To address these concerns, researchers have sought alternative elements to replace Pb in perovskite structures.[20,21] Some groups encountered the challenge of increased band gap values when substituting Pb with alkaline earth metals, rendering the resulting band gaps (>3.1 eV) unsuitable for visible light absorption, and several other researchers explored substitutions with Sn and Ge, but this exacerbated the instability issue.[22]

To overcome the problems of toxicity and instability, the use of halide double perovskites in the form of $A_2BB'X_6$ (where A represents large cations like divalent alkaline earth elements, B and B′ represent small cations mostly from transition-metal elements, and X is anion) has emerged as a promising alternative. In this context, ongoing research efforts are focused on achieving optimal material growth design for solar cells and other applications. Computer simulations are widely used to guide researchers in modeling the best methods that meet the desired goals. Therefore, we are motivated to investigate the physical properties of the halide double perovskites K_2BCuCl_6 (B = Sc, and Y) using computer simulations, explicitly focusing on their suitability for solar cells. Our study aims to explore the density of states (DOS), band structure, and optical properties, i.e., reflectivity, refractivity, and optical conductivity, as well as these materials' structural and elastic properties.

2. COMPUTATIONAL METHODOLOGY

Density functional theory (DFT) is a versatile approach widely utilized to investigate the characteristics of materials before their practical implementation.[23] This computational tool provides information about various material properties, essential for understanding their behavior and optimizing their performance for practical manufacturing.[24] In this study, we employ the WIEN2K code[25] and the full potential linearized augmented plane wave method to perform computations on K_2BCuCl_6 (B =

Sc, and Y) compounds.[26] To determine the optimized lattice parameters and system energy, we incorporate Murnaghan's equations of state (EoS).[27] The TB-mBJ potential, renowned for its simplicity and accuracy, is employed to calculate the band gaps.[28] It has demonstrated comparable results to the computationally investigated HSE0$_6$ hybrid functional.[29] Ensuring convergence of charge and energy is crucial for the accuracy of the calculated results; therefore, a larger K-mesh of 2000 is employed. The −6.0 Ry in WIEN2K specifies the energy below, treated as core states, where core electrons are assumed to not to interact. The valence electrons of all constituent elements are considered for our calculations. The atomic configuration of constituent elements is; potassium (K) is $1s^2$, $2s^2$, $2p^6$, $3s^2$, $3p^6$, and $4s^1$, for scandium (Sc) is $1s^2$, $2s^2$, $2p^6$, $3s^2$, $3p^6$, $3d^1$, and $4s^2$, for yttrium (Y) is $1s^2$, $2s^2$, $2p^6$, $3s^2$, $3p^6$, $3d^{10}$, $4s^2$, $4p^6$, and $4d^1$, for copper (Cu) is $1s^2$, $2s^2$, $2p^6$, $3s^2$, $3p^6$, $4s^1$, and $3d^{10}$, and that for chlorine (Cl) is $1s^2$, $2s^2$, $2p^6$, $3s^2$, and $3p^5$. To enhance the clarity of our research, we have systematically incorporated phonon calculations by employing a well-established and effective finite displacement method. This approach was implemented using the phonopy code,[30] and to ensure accurate and reliable results, we employed a $4 \times 6 \times 3$ supercell selection. The calculations were performed using the Vienna ab initio Simulation Packages as our computational tool.[31] This meticulous combination of methods and tools allowed us to thoroughly investigate the vibrational properties of our system.

3. RESULTS AND DISCUSSION

3.1. Structural Properties. The cubic structures of the double perovskites K_2BCuCl_6 (B = Sc and Y) can be visualized as combinations of two simple perovskite structures belonging to the $Fm\overline{3}m$ (225) space group. As shown in Figure 1, the polyhedral shape of the K_2BCuCl_6 (B = Sc and Y) reveals the formation of octahedra, with each atom being surrounded by six Cl atoms; i.e., atoms of Sc/Y octahedra and Cu octahedra are positioned within the structure, with Cl atoms surrounding them.

The atoms K, Sc/Y, Cu, and Cl occupy specific Wyckoff positions of (1/4, 3/4, 3/4), (0, 0, 0), (1/2, 0, 0) and (0.24, 0, 0)/(0.274, 0, 0), respectively. The optimized parameters for the unit cell and the positions of the atoms are briefly presented in Table 1.

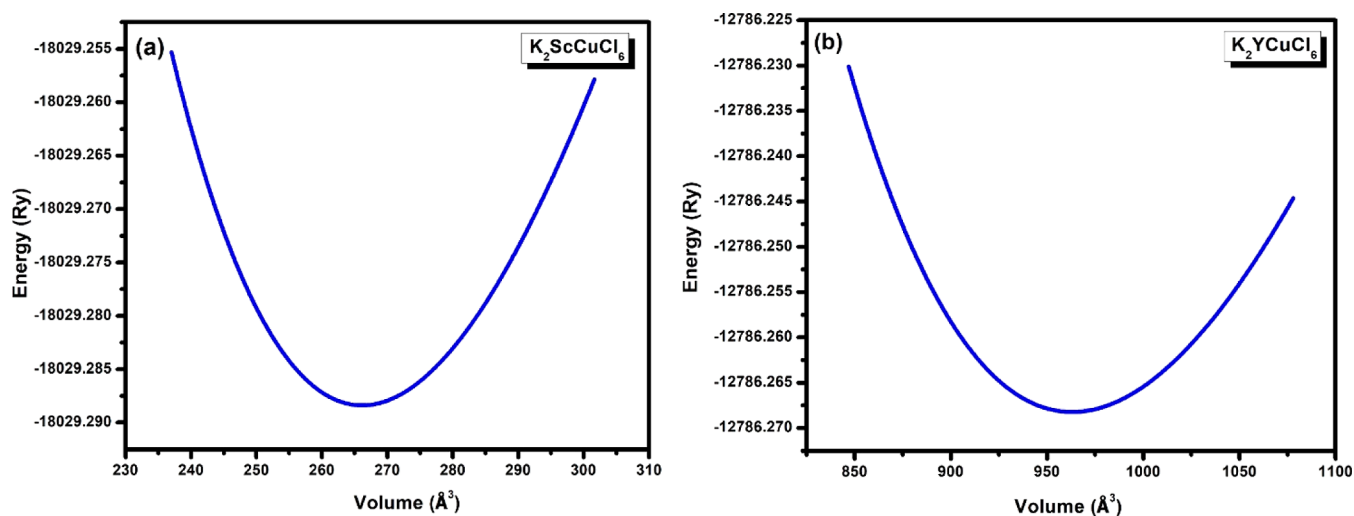The optimization process is utilized to minimize the energy of the unit cell for both compounds. To achieve this, Birch−

Figure 2. Volume optimization graphs of (a) $K_2ScCuCl_6$ and (b) K_2YCuCl_6.

Murnaghan's EoS is employed. The results of the volume optimization for the double perovskite compounds are depicted in Figure 2. The figure illustrates parabolic curves that represent the relationship between energy and volume. The minimum points on these curves correspond to the ground state of the compounds, indicating their most stable configuration.

Table 2 presents an overview of the structural parameters, particularly B_0, B', and a_0, which play a crucial role in

Table 2. Calculated Optimized Structural Parameters of $K_2ScCuCl_6$ and K_2YCuCl_6

compounds	a_0 (Å)	B (GPa)	B' (GPa)	E_0 (Ry)
$K_2ScCuCl_6$	10.25	32.98	2.05	−12786.26
K_2YCuCl_6	10.30	34.68	0.39	−18029.28

understanding the structural characteristics of the double perovskite compounds. The values of B_0 and B' are comparable to those reported for other halogen perovskites.[32] The values of B' are much smaller than 4, which means that compressibility will increase little with pressure, and thus, the volume–pressure relationship is quasi-linear.[33,34]

3.2. Phonon Stability. To gain an understanding of the dynamic context, including vibrational Raman spectroscopy of crystalline solids and thermodynamic characteristics, it is essential to take into account the phonon dispersion.[35] To accomplish this, a widely utilized and effective method is the DFPT implemented in the pseudopotential scheme of Quantum

Espresso.[36] By employing DFPT on the perovskite structures of $K_2ScCuCl_6$ and K_2YCuCl_6, one can examine their dynamic stability within their respective primitive unit cells. When analyzing the molecular structures of crystals in terms of their dynamic characteristics, a compound is considered dynamically stable when it exhibits three acoustic branches at the Γ-point in reciprocal space, with frequencies of zero. These acoustic branches consist of one longitudinal acoustic mode and two transverse acoustic modes. Conversely, the remaining branches, referred to as optical phonons, possess nonzero frequencies. In a crystal with N atoms in its unit cell, there are typically 3N−3 optical modes. Therefore, in the context of this particular study, which involves 10 constituent atoms, there exist a total of 30 frequency branches. Within these branches, three acoustic branches converge at the Γ-point, while the remaining 27 branches exhibit optical characteristics, as illustrated in Figure 3. Notably, the lower branches predominantly stem from the vigorous vibrations of the heavier elements, whereas the optical branches primarily correspond to the lighter atoms. Based on factor theory, the optical branches encompass various modes, including Raman, infrared, and silent modes, depending on their frequency range.

The absence of negative or imaginary frequencies observed in the subsequent band dispersions confirms the dynamic stability observed in the studied systems. This observation is similar to the results reported by Ding et al.,[37] implying that the perovskite
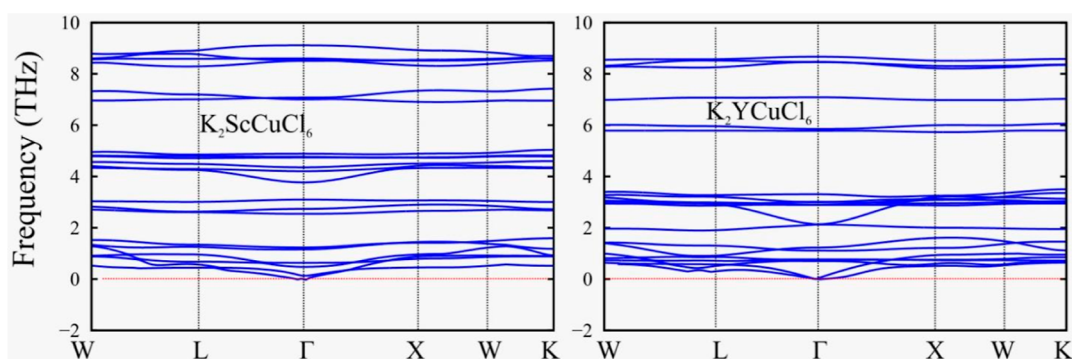

Figure 3. Phonon band structures within the irreducible BZ of the primitive unit cell structures of $K_2ScCuCl_6$ and K_2YCuCl_6.

structures of $K_2ScCuCl_6$ and K_2YCuCl_6 exhibit reliable and stable vibrational characteristics.

3.3. Elastic Properties. The mechanical stability of a crystal structure is a crucial aspect to consider when assessing the behavior of a material under stress. Mechanical stability can be determined by examining the elastic constants, which describe the material's response to applied forces. For materials with cubic symmetry, e.g., the double perovskite compounds under investigation, three specific elastic constants are essential: C_{11}, C_{12}, and C_{44}. These constants must satisfy the Born stability criteria to ensure that the crystal structure is mechanically stable.[38,39] Furthermore, the ductility or brittleness of a material is an important characteristic that influences its potential applications. Poisson's ratio (v) measures a material's tendency to undergo lateral deformation when subjected to an axial strain. A value greater than 0.26 is typically indicative of ductile behavior. Similarly, the Pugh ratio, defined as the ratio of the bulk modulus (B) to the shear modulus (G), can provide insights into the material's flexibility. A Pugh ratio B/G exceeding 1.75 is generally associated with ductile materials.[40]

From the data presented in Table 2, it can be observed that the studied double perovskite compounds exhibit a ductile nature. This suggests that they possess favorable mechanical properties for use in device fabrications. Furthermore, the values of B show that the studied compounds are extremely compressible than other perovskites.[41] The studied compounds are among the most compressible solids with a B comparable to iodates.[42] Additionally, anisotropy, which characterizes the directional dependence of the material properties, is another crucial factor to consider. Anisotropy can be quantified by the relationship $A = 2C_{44}/(C_{11} - C_{12})$, where C_{44}, C_{11}, and C_{12} represent specific elastic constants. The anisotropic behavior of the compounds can be determined based on the calculated values presented in Table 3. For instance, K_2YCuCl_6 exhibits a higher anisotropy compared to $K_2ScCuCl_6$.

Table 3. Calculated Elastic Parameters A, B, G, E (All in GPa), v, and B/G of $K_2ScCuCl_6$ and K_2YCuCl_6

compounds	A	B	G	E	V	B/G
$K_2ScCuCl_6$	0.77	40.8	16.86	43.23	0.39	1.95
K_2YCuCl_6	1.07	33.03	15.17	39.73	0.43	2.28

The values of B derived from the volumetric strain versus pressure ($E-V$) relationship are observed to be consistently lower than those obtained through the analysis of the elastic constants. This discernible discrepancy may be attributed to using distinct measurement techniques in the two methodologies.

By investigating the elastic behavior of the double perovskite compounds and considering factors, i.e., mechanical stability, flexibility, and anisotropy, we can gain valuable insights into their potential applications and suitability for specific engineering purposes.

3.4. Electronic Properties. This section explores the calculation of band structures and DOS for double perovskite compounds, specifically, $K_2ScCuCl_6$ and K_2YCuCl_6. The analysis of band structures offers valuable insights into the conductivity characteristics of these materials, establishing a connection between their crystal structures and optical/electronic properties.

Figure 4 presents the band structures of $K_2ScCuCl_6$ and K_2YCuCl_6 compounds, which are computed by using the TB-

mBJ potential. It is evident from the figure that both the compounds demonstrate a semiconducting behavior, characterized by band gaps of 1.8 and 2.5 eV, respectively.

As we progress from $K_2ScCuCl_6$ to K_2YCuCl_6 by substituting Sc for Y, the band gap value increases. This phenomenon can be attributed to the larger atomic size of Y. Consequently, the conduction band minimum moves farther from the Fermi level, resulting in an enlarged band gap. We anticipate that the values we have reported will inspire experimental researchers, encouraging them to fabricate these materials for the production of solar cells. DOS calculation provides a detailed analysis of electronic properties, confirming and understanding the band gap. It characterizes energy state distribution and reveals the nature of the band gap, aiding in understanding electronic behavior.[43,44] The Fermi energy (E_F) represents the boundary between the valence and conduction bands, with the valence band containing occupied low-energy levels and the conduction band consisting of unoccupied levels above E_F.

In the plots (Figure 5), the valence band is mainly contributed by Cu and halogen atoms (Cl), while Y/Sc and halogen atoms primarily influence the conduction band. This suggests that the occupied energy levels originate from Cu and halogen orbitals, while unoccupied levels and electron conduction arise from Y/Sc orbitals. A comparable trend in the DOS was identified in the study conducted by Vu et al.[45]

3.5. Optical Properties. Optical properties of materials involve their interaction with light and are vital in optics, photonics, and optoelectronics. Fundamental properties include the refractive index, optical conductivity, refraction, reflection, extinction, absorption, loss, and dielectric function. Figure 6 shows the computed $\varepsilon_1(\omega)$ and $\varepsilon_2(\omega)$ for two materials within the range of incident photon energy up to 14 eV. $\varepsilon_1(\omega)$ represents energy dissipation and wave damping, while $\varepsilon_2(\omega)$ is associated with polarization and energy storage. The static dielectric function, $\varepsilon_1(0)$, indicates that $K_2ScCuCl_6$ dissipates more energy (2.8) compared to K_2YCuCl_6 (2.5). Both compounds exhibit maximum values of $\varepsilon_2(\omega)$: 3.6 at 12.9 eV and 2.7 at 6.5 eV, respectively.

The refractive index measures how light travels through a material and is influenced by the composition and structure. The refractive index of a material can be calculated using the values of $\varepsilon_1(\omega)$ and $\varepsilon_2(\omega)$ obtained from the dielectric function. Figure 7a illustrates the refractive indexes for $K_2ScCuCl_6$ and K_2YCuCl_6. The static refractive index values, $n(0)$, are 1.65 for $K_2ScCuCl_6$ and 1.58 for K_2YCuCl_6. The spectrum of $n(\omega)$ shows that $K_2ScCuCl_6$ reaches a peak value of 2.1 at around 5.6 eV, while K_2YCuCl_6 exhibits a maximum peak value of 2.02 at approximately 2.8 eV of photon energy. The static refractive index, $n(0)$, is valuable in applications related to light refraction, particularly in photoelectric applications. When $n(\omega)$ is greater than 1, it indicates that photons slow as they enter a material and interact with electrons, resulting in a more significant delay for the photons passing through the substance. Increasing the electronic density of a material also leads to a higher refractive index $n(\omega)$.

Figure 7b shows the computed reflectivity $R(\omega)$ for the double perovskite compounds $K_2ScCuCl_6$ and K_2YCuCl_6. $K_2ScCuCl_6$ has a reflectivity of 0.058 at zero frequency $R(0)$, while K_2YCuCl_6 has a value of 0.051. As the photon energy increases, the reflectivity of both compounds also increases. They reach maximum reflectivity values of 0.59 and 0.56 at around 13.5 eV, respectively. Both compounds, $K_2ScCuCl_6$ and K_2YCuCl_6, exhibit remarkably low reflectivity within the
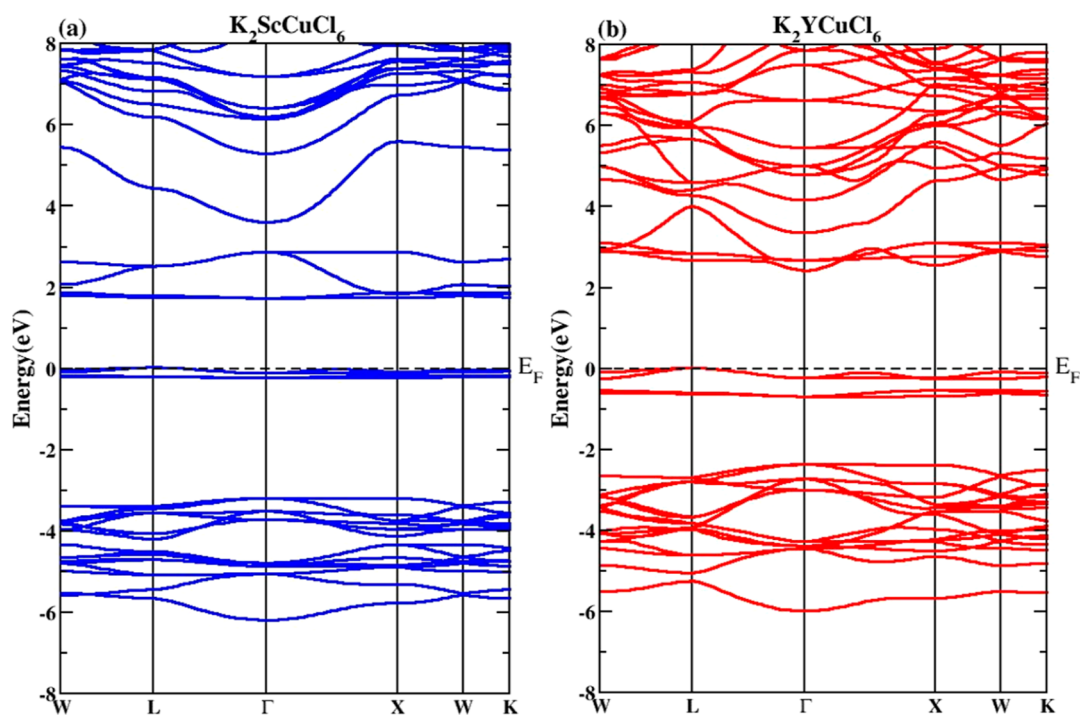
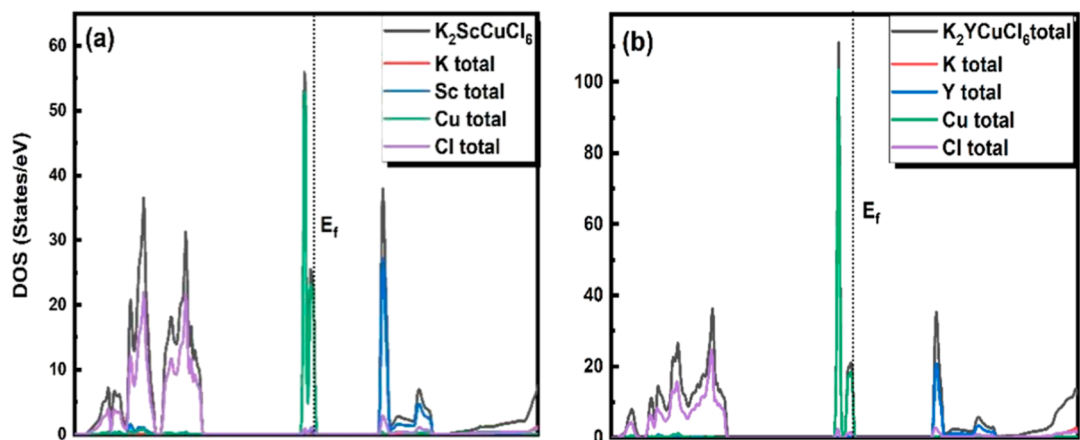**Figure 4.** Calculated TDOS of double perovskites (a) $K_2ScCuCl_6$ and (b) K_2YCuCl_6.

Figure 5. Calculated DOS of double perovskites $K_2ScCuCl_6$ and K_2YCuCl_6.
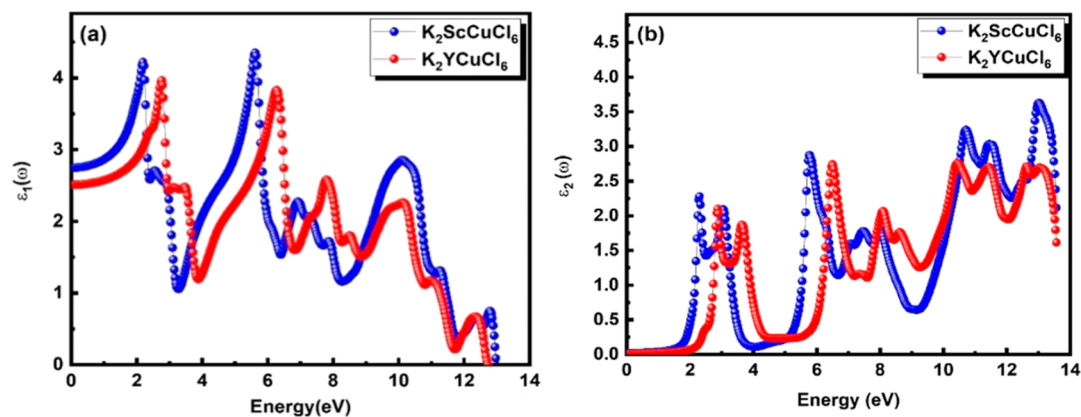

Figure 6. Calculated (a) $\varepsilon_1(\omega)$ and (b) $\varepsilon_2(\omega)$ of double perovskites $K_2ScCuCl_6$ and K_2YCuCl_6.

measured energy range. This low reflectivity is consistent with their band gap, making them highly transparent to incoming photons. The high transparency of these materials makes them promising for applications in solar cells and lenses, where the
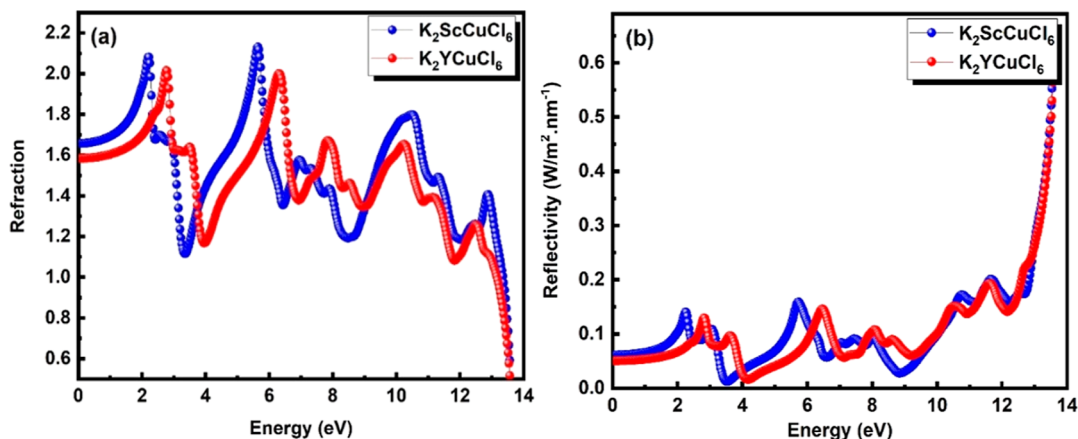
Figure 7. Calculated (a) refractive index $n(\omega)$ and (b) reflectivity $R(\omega)$ of $K_2ScCuCl_6$ and K_2YCuCl_6.
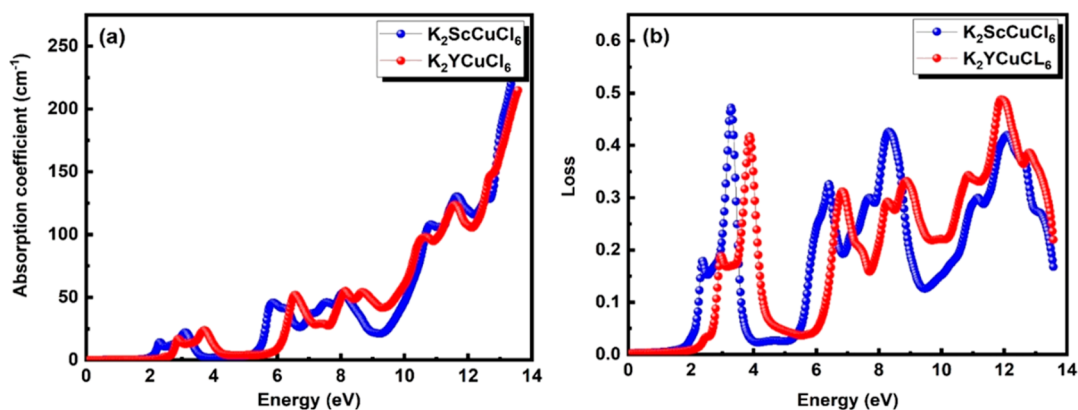

Figure 8. Calculated (a) $\alpha(\omega)$ and (b) $L(\omega)$ of double perovskites $K_2ScCuCl_6$ and K_2YCuCl_6.
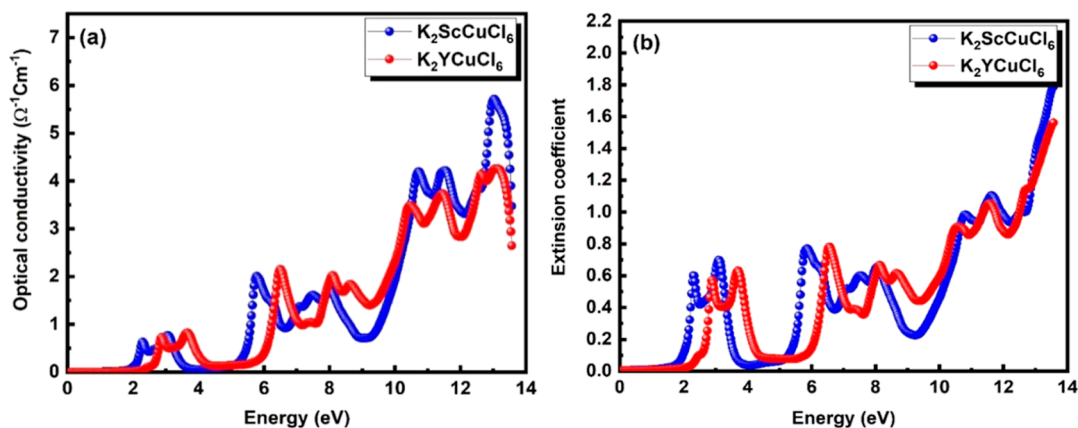

Figure 9. Calculated (a) $\sigma(\omega)$ and (b) $k(\omega)$ of double perovskites $K_2ScCuCl_6$ and K_2YCuCl_6.

ability to transmit light efficiently is desirable. Figure 8a presents the absorption curves obtained through the $\varepsilon(\omega)$ approach for the selected compounds $K_2ScCuCl_6$ and K_2YCuCl_6. These compounds exhibit significant absorption within the 0 to 14 eV. The threshold points of absorption occur at 0 eV, indicating the starting point at which these substances begin to absorb electromagnetic radiation. At a photon energy of 13.5 eV, $K_2ScCuCl_6$ demonstrates a maximum absorption value of 246.3, while K_2YCuCl_6 exhibits a maximum absorption of 215.9. This indicates the efficiency with which these compounds can absorb light in a specified energy range.

Figure 8b depicts the energy loss function, which describes the energy loss of fast electrons in a material. The peaks in the $L\omega$ spectra correspond to characteristic features related to the plasma resonance. $K_2ScCuCl_6$ exhibits a distinct resonant energy loss at 3.26 eV, while K_2YCuCl_6 shows it at 1.8 eV. These resonant peaks signify significant energy dissipation in the materials. Analyzing the energy loss function provides valuable insights into electron behavior and material interaction, offering essential information for understanding phenomena and applications in solid-state physics and materials science.

Figure 9a shows that $K_2ScCuCl_6$ has a maximum optical conductivity value of approximately 5.75 Ω^{-1} cm^{-1}, while

K_2YCuCl_6 exhibits a significant value of roughly 4.29 Ω^{-1} cm^{-1}. This indicates that these compounds have excellent optical conductivity, especially at higher energies. Their favorable optical conductivity characteristics make them promising candidates for applications in photonics, telecommunications, and other emerging optoelectronic technologies. The extinction coefficient measures how much light is absorbed and scattered in a material. A higher value indicates stronger absorption and scattering, reducing transmission, and increasing attenuation. $K_2ScCuCl_6$ has a maximum extinction coefficient of 1.79, while K_2YCuCl_6 has a leading extinction coefficient of 1.56.

4. CONCLUSIONS

In the scope of this study, a thorough exploration was conducted into the optoelectronic, structural, optical, and elastic properties of the double perovskite compounds $K_2ScCuCl_6$ and K_2YCuCl_6, utilizing DFT calculations. The findings unveil structural stability, mechanical resilience, anisotropy, toughness, and resistance to plastic deformation in both compounds. The assurance of structural and phonon stability is underscored by the absence of negative energy formations and the presence of exclusively real frequencies in the phonon calculations. Moreover, the application of DFT substantiates all compounds' thermodynamic stability. The assessment of structural stability is further refined using Goldsmith's stability index, where values nearing unity signify a robust cubic perovskite structure. The electronic properties are meticulously unraveled through the precise TB-mBJ approximation, revealing narrow band gaps of 1.8 and 2.5 eV for $K_2ScCuCl_6$ and K_2YCuCl_6, respectively. Optical analyses shed light on transparency at lower photon energies and noteworthy absorption and transmission at higher energy levels, providing a comprehensive understanding of the compounds' behavior in various aspects of their properties.

ASSOCIATED CONTENT

Data Availability Statement

The data used to support the findings of this study are available from the corresponding author upon request.

AUTHOR INFORMATION

Corresponding Authors

Nasir Rahman — *Department of Physics, University of Lakki Marwat, Lakki Marwat, Khyber Pakhtunkhwa 28420, Pakistan;* orcid.org/0000-0003-1978-7280; Email: nasir@ulm.edu.pk

Aurangzeb Khan — *Department of Physics, Abdul Wali Khan University, Mardan 23200, Pakistan;* Email: akhan@awkum.edu.pk

Authors

Saima Ahmad Shah — *Department of Physics, Abdul Wali Khan University, Mardan 23200, Pakistan; Department of Physics, Shaheed Benazir Bhutto Women University, Peshawar 00384, Pakistan*

Mudasser Husain — *State Key Laboratory for Mesoscopic Physics and Department of Physics, Peking University, Beijing 100871, P. R. China*

Nourreddine Sfina — *College of Sciences and Arts in Mahayel Asir, Department of Physics, King Khalid University, Abha 61413, Saudi Arabia*

Muawya Elhadi — *Department of Physics, Faculty of Science and Humanities, Shaqra University, Ad-Dawadimi 11911, Saudi Arabia*

Vineet Tirth — *Mechanical Engineering Department, College of Engineering, King Khalid University, Abha, Asir 61421, Kingdom of Saudi Arabia; Centre for Engineering and Technology Innovations, King Khalid University, Abha 61421, Kingdom of Saudi Arabia;* orcid.org/0000-0002-8208-7183

Afraa Alotaibi — *Department of Physics, College of Science, Princess Nourah bint Abdulrahman University, Riyadh 11671, Saudi Arabia*

Complete contact information is available at: https://pubs.acs.org/10.1021/acsomega.4c01923

Notes

The authors declare no competing financial interest.

ACKNOWLEDGMENTS

REFERENCES

(1) Wang, D.; Wang, X.-X.; Jin, M. L.; He, P.; Zhang, S. Molecular level manipulation of charge density for solid-liquid TENG system by proton irradiation. *Nano Energy* **2022**, *103*, 107819.

(2) Wang, M.; Jiang, C.; Zhang, S.; Song, X.; Tang, Y.; Cheng, H.-M. Reversible calcium alloying enables a practical room-temperature rechargeable calcium-ion battery with a high discharge voltage. *Nat. Chem.* **2018**, *10* (6), 667−672.

(3) Chen, X.-F. Periodic Density Functional Theory (PDFT) Simulating Crystal Structures with Microporous CHA Framework: An Accuracy and Efficiency Study. *Inorganics* **2023**, *11* (5), 215.

(4) Zhang, X.; Tang, Y.; Zhang, F.; Lee, C. A novel aluminum-graphite dual-ion battery. *Adv. Energy Mater.* **2016**, *6* (11), 1502588.

(5) Chen, X.; Yu, T. Simulating Crystal Structure, Acidity, Proton Distribution, and IR Spectra of Acid Zeolite HSAPO-34: A High Accuracy Study. *Molecules* **2023**, *28* (24), 8087.

(6) Ye, S.; Zhu, J.; Zhu, S.; Zhao, Y.; Li, M.; Huang, Z.; Wang, H.; He, J. Design Strategies for Perovskite-Type High-Entropy Oxides with Applications in Optics. *ACS Appl. Mater. Interfaces* **2023**, *15* (40), 47475−47486.

(7) Wang, Z.; Fu, W.; Hu, L.; Zhao, M.; Guo, T.; Hrynsphan, D.; Tatsiana, S.; Chen, J. Improvement of electron transfer efficiency during denitrification process by Fe-Pd/multi-walled carbon nanotubes: Possessed redox characteristics and secreted endogenous electron mediator. *Sci. Total Environ.* **2021**, *781*, 146686.

(8) Luo, Z.-Z.; Cai, S.; Hao, S.; Bailey, T. P.; Luo, Y.; Luo, W.; Yu, Y.; Uher, C.; Wolverton, C.; Dravid, V. P.; et al. Extraordinary role of Zn in enhancing thermoelectric performance of Ga-doped n-type PbTe. *Energy Environ. Sci.* **2022**, *15* (1), 368−375.

(9) Zhu, Q.; Chen, J.; Gou, G.; Chen, H.; Li, P. Ameliorated longitudinal critically refracted—Attenuation velocity method for welding residual stress measurement. *J. Mater. Process. Technol.* **2017**, *246*, 267−275.

(10) Zhu, L.; Li, Z.; Hou, K. Effect of radical scavenger on electrical tree in cross-linked polyethylene with large harmonic superimposed DC voltage. *High Voltage* **2023**, *8* (4), 739−748.

(11) Song, X.; Yang, S.; Wang, G.; Lin, J.; Wang, L.; Meier, T.; Yang, W. Control of the electron dynamics in solid-state high harmonic generation on ultrafast time scales by a polarization-skewed laser pulse. *Opt. Express* **2023**, *31* (12), 18862−18870.

(12) Lu, Y.; Stegmaier, M.; Nukala, P.; Giambra, M. A.; Ferrari, S.; Busacca, A.; Pernice, W. H. P.; Agarwal, R. Mixed-mode operation of hybrid phase-change nanophotonic circuits. *Nano Lett.* **2017**, *17* (1), 150−155.

(13) Husain, M.; Rahman, N.; Azzouz-Rached, A.; Tirth, V.; Ullah, H.; Elhadi, M.; Uzair, M.; Alotaibi, A.; Humayun, Q.; Sfina, N.; et al. Exploring Silicon-Based Ca2TiSiO6 Ordered Double Perovskite Oxides: a Comprehensive DFT Investigation of Structural, Dynamical, Mechanical Stability, and Optoelectronic Properties. *Silicon* **2024**, 1−4.

(14) Bibi, S.; Husain, M.; Tirth, V.; Ben Ahmed, S.; Rahman, N.; Azzouz-Rached, A.; Ullah, H.; Khan, M. Y.; Khan, A. Insight into the physical properties of Rb2YCuX6 (X = Br and I) lead-free elpasolite for high-energy applications. *Phys. Scr.* **2024**, *99*, 035906.

(15) Rahman, N.; Husain, M.; Tirth, V.; Azzouz-Rached, A.; Bibi, S.; Inayat, K.; Khan, R.; Sohail, M.; Ullah, H.; Nasir, M.; et al. Insight into the structural, elastic, phonon dispersions, and optoelectronic properties of Cs2YXCl6 (X = In, Tl) double perovskites for solar cells and energy conversion applications. *Optik* **2024**, *299*, 171590.

(16) Lu, C.; Ren, R.; Zhu, Z.; Pan, G.; Wang, G.; Xu, C.; Qiao, J.; Sun, W.; Huang, Q.; Liang, H.; et al. BaCo0.4Fe0.4Nb0. 1Sc0. 1O3-δ perovskite oxide with super hydration capacity for a high-activity proton ceramic electrolytic cell oxygen electrode. *Chem. Eng. J.* **2023**, *472*, 144878.

(17) Huang, Z.; Zhang, Y.; Wang, H.; Li, J. Improved electrical resistivity-temperature characteristics of oriented hBN composites for inhibiting temperature-dependence DC surface breakdown. *Appl. Phys. Lett.* **2023**, *123* (10), 103501.

(18) Jiang, C.; Deng, Z.; Liu, B.; Li, J.; Han, Z.; Ma, Y.; Wu, D.; Maeda, H.; Ma, Y. Spin-Orbit-Engineered Selective Transport of Photons in Plasmonic Nanocircuits with Panda-Patterned Transporters. *ACS Photonics* **2022**, *9* (9), 3089−3093.

(19) Kong, L.; Liu, Y.; Dong, L.; Zhang, L.; Qiao, L.; Wang, W.; You, H. Enhanced red luminescence in CaAl 12 O 19: Mn 4+ via doping Ga 3+ for plant growth lighting. *Dalton Trans.* **2020**, *49* (6), 1947−1954.

(20) Rahman, N.; Rauf, A.; Husain, M.; Sfina, N.; Tirth, V.; Sohail, M.; Khan, R.; Azzouz-Rached, A.; Murtaza, G.; Khan, A. A.; et al. Probing the physical properties of M 2 LiCeF 6 (M = Rb and Cs) double perovskite compounds for prospective high-energy applications employing the DFT framework. *RSC Adv.* **2023**, *13* (23), 15457−15466.

(21) Shah, S. A.; Husain, M.; Tirth, V.; Azzouz-Rached, A.; Rahman, N.; Khan, A. First-principles calculations to investigate the structural, electronic, optical, mechanical, and thermodynamic properties of double perovskites Ba2WB′ O6 (B′= Co, Fe, Mn, Ni, and Zn). *Optik* **2024**, *300*, 171636.

(22) Jehan, A.; Husain, M.; Tirth, V.; Algahtani, A.; Uzair, M.; Rahman, N.; Khan, A.; Khan, S. N. Investigation of the structural, electronic, mechanical, and optical properties of NaXCl 3 (X= Be, Mg) using density functional theory. *RSC Adv.* **2023**, *13* (41), 28395−28406.

(23) Obot, I. B.; Macdonald, D. D.; Gasem, Z. M. Density functional theory (DFT) as a powerful tool for designing new organic corrosion inhibitors. Part 1: an overview. *Corros. Sci.* **2015**, *99*, 1−30.

(24) Hafner, J.; Wolverton, C.; Ceder, G. Toward computational materials design: the impact of density functional theory on materials research. *MRS Bull.* **2006**, *31* (9), 659−668.

(25) Blaha, P.; Schwarz, K.; Madsen, G. K. H.; Kvasnicka, D.; Luitz, J. *WIEN2K: An Augmented Plane Wave Plus Local Orbitals Program for Calculating Crystal Properties*; Vienna University of Technology: Vienna, Austria, 2001.

(26) Blaha, P.; Schwarz, K.; Sorantin, P.; Trickey, S. B. Full-potential, linearized augmented plane wave programs for crystalline systems. *Comput. Phys. Commun.* **1990**, *59* (2), 399−415.

(27) Katsura, T.; Tange, Y. A simple derivation of the Birch-Murnaghan equations of state (EOSs) and comparison with EOSs derived from other definitions of finite strain. *Minerals* **2019**, *9* (12), 745.

(28) Kadim, G.; Masrour, R.; Jabar, A. A comparative study between GGA, WC-GGA, TB-mBJ and GGA+ U approximations on magneto-caloric effect, electronic, optic and magnetic properties of BaMnS2 compound: DFT calculations and Monte Carlo simulations. *Phys. Scr.* **2021**, *96* (4), 045804.

(29) Schimka, L.; Harl, J.; Kresse, G. Improved hybrid functional for solids: The HSEsol functional. *J. Chem. Phys.* **2011**, *134* (2), 024116.

(30) Togo, A. First-principles phonon calculations with phonopy and phono3py. *J. Phys. Soc. Jpn.* **2023**, *92* (1), 12001.

(31) Hafner, J. Ab-initio simulations of materials using VASP: Density-functional theory and beyond. *J. Comput. Chem.* **2008**, *29* (13), 2044−2078.

(32) Khawar, S.; Afzal, M. Q.; Husain, M.; Sfina, N.; Albalawi, H.; Naeem, M. A.; Rahman, N.; Amami, M.; Khan, R.; Sohail, M.; et al. First-principles calculations to investigate structural, electronic, optical, and magnetic properties of a scintillating double perovskite halide (Cs2LiCeCl6). *J. Mater. Res. Technol.* **2022**, *21*, 4790−4798.

(33) Hofmeister, A. M. Pressure derivatives of the bulk modulus. *J. Geophys. Res.: Solid Earth* **1991**, *96* (B13), 21893−21907.

(34) Anzellini, S.; Errandonea, D.; Cazorla, C.; MacLeod, S.; Monteseguro, V.; Boccato, S.; Bandiello, E.; Anichtchenko, D. D.; Popescu, C.; Beavers, C. M. Thermal equation of state of ruthenium characterized by resistively heated diamond anvil cell. *Sci. Rep.* **2019**, *9* (1), 14459.

(35) Togo, A.; Tanaka, I. First principles phonon calculations in materials science. *Scr. Mater.* **2015**, *108*, 1−5.

(36) Giannozzi, P.; Baroni, S.; Bonini, N.; Calandra, M.; Car, R.; Cavazzoni, C.; Ceresoli, D.; Chiarotti, G. L.; Cococcioni, M.; Dabo, I.; et al. QUANTUM ESPRESSO: a modular and open-source software project for quantum simulations of materials. *J. Phys.: Condens. Matter* **2009**, *21* (39), 395502.

(37) Ding, G.; Xie, C.; Bai, J.; Cheng, Z.; Wang, X.; Wu, W. Recipe for single-pair-Weyl-points phonons carrying the same chiral charges. *Phys. Rev. B* **2023**, *108*, L020302.

(38) Milstein, F.; Zhao, J.; Chantasiriwan, S.; Maroudas, D. Applicability of Born's stability criterion to face-centered-cubic crystals in [111] loading. *Appl. Phys. Lett.* **2005**, *87* (25), 251919.

(39) Zhang, Y.; Liu, X.; Song, M.; Qin, Z. Tuning the Red-to-Green-Upconversion Luminescence Intensity Ratio of Na3ScF6: 20% Yb3+, 2% Er3+ Particles by Changes in Size. *Materials* **2023**, *16* (6), 2247.

(40) Pugh, S. F. XCII. Relations between the elastic moduli and the plastic properties of polycrystalline pure metals. *London, Edinburgh, Dublin Philos. Mag. J. Sci.* **1954**, *45* (367), 823−843.

(41) Qiu, Y.; Shi, M.; Guo, X.; Li, J.; Wu, J.; Zhou, Y.; Sun, H.; Hang, Y.; Li, X.; Li, Y. Sensitivity improvement in the measurement of minor components by spatial confinement in fiber-optic laser-induced breakdown spectroscopy. *Spectrochim. Acta, Part B* **2023**, *209*, 106800.

(42) Qiu, Y.; Guo, X.; Shi, M.; Zhou, Y.; Wu, J.; Li, J.; Sun, H.; Zhang, Z.; Hang, Y.; Li, X.; et al. Plasma dynamics and chlorine emission characteristics on cement pastes using collinear dual-pulse laser-induced breakdown spectroscopy. *Spectrochim. Acta, Part B* **2023**, *209*, 106799.

(43) Du, S.; Yin, J.; Xie, H.; Sun, Y.; Fang, T.; Wang, Y.; Li, J.; Xiao, D.; Yang, X.; Zhang, S.; et al. Auger scattering dynamic of photo-excited hot carriers in nano-graphite film. *Appl. Phys. Lett.* **2022**, *121* (18), 181104.

(44) Lyu, J.; Huang, L.; Chen, L.; Zhu, Y.; Zhuang, S. Review on the terahertz metasensor: from featureless refractive index sensing to molecular identification. *Photonics Res.* **2024**, *12* (2), 194−217.

(45) Vu, T. V.; Lavrentyev, A. A.; Gabrelian, B. V.; Vo, D. D.; Pham, K. D.; Denysyuk, N. M.; Isaenko, L. I.; Tarasova, A. Y.; Khyzhun, O. Y. DFT study and XPS measurements elucidating the electronic and optical properties of KPb2Cl5. *Opt. Mater.* **2020**, *102*, 109793.